This article was published in Physical Chemistry Chemical Physics, 17(35), 22699-22710, 2015
http://dx.doi.org/10.1039/c5cp02942b

Temperature Role in the Recombination Reaction on Dye-Sensitized Solar Cells

J. Maçaira[a], I. Mesquita[a], L. Andrade[a] and A. Mendes[a]

[a] LEPABE – Faculdade de Engenharia, Universidade do Porto, rua Dr. Roberto Frias,
4200-465, Portugal. E-mail: mendes@fe.up.pt

The performance of photovoltaic (PV) devices as a function of temperature is crucial for technical development and for accurate commercial information. Along with solar irradiance, temperature is the most important operating factor of PV devices performance. Normally it is wide accepted that dye sensitized solar cells (DSC) show minimal energy efficiency dependence with temperature (20 °C – 60 °C). The energy efficiency in DSCs depends on light absorption, charge transport (ohmic resistances) and recombination rates. In this work the recombination reaction kinetics is studied within a wide temperature range. A unique laser assisted sealing technique that allows studying the temperature effect between -5 ºC and 105 ºC without electrolyte leakage or external contamination was used. To the best of our knowledge, this is the highest operating temperature ever considered in kinetic studies of liquid state DSCs. The electrochemical reaction between electrons and triiodide/iodide ions is shown to be the most important factor to determine the energy efficiency of DSCs as a function of temperature. It was concluded that the activation energy of the recombination reactions depends on the interface where it happens – TiO_2/electrolyte and SnO_2-F/electrolyte – and on the temperature. It was found that besides temperature having a deep influence in the recombination reaction rate, the energy of the injecting electron is also critical. These conclusions should provide solid ground for further developments in the DSCs and perovskite solar cell fields, and allow a better comparison between the energy efficiency of different PV technologies for a range of operating temperatures.

1. Introduction

Direct conversion of solar light into electricity is becoming a winning strategy with photovoltaic (PV) electricity cost, already below the grid in several countries[1]. However, high production costs prevent the current PV solutions from standing out as a real energy production alternative. Dye-sensitized solar cells (DSCs) are an important type of thin-film photovoltaics due to their potential for low-cost fabrication and versatile applications and are already looked upon as a future alternative to silicon PV devices. The presumed cost/effectiveness of DSCs makes them worth investing [2-4]. Regardless the countless efforts and enormous amount of publications[5] the maximum photo conversion efficiency (η) of DSCs has been stagnated in the range of 12 % [6-8] over the last ten years. The best conversion efficiency of a DSC device was achieved using porphyrin-sensitizers coupled with cobalt (II/III) based redox electrolyte under simulated air mass 1.5 global sunlight (AM 1.5G) conditions (100 $mW{\cdot}cm^{-2}$)[9]. Recently, lead halide perovkite absorber combined with a solid hole transporting material (HTM) have ramped up efficiencies from 14.1 % [10] in 2013 to an impressive certified result of 20.1 % in the early of 2015 [11, 12]. Although DSCs and perovskite solar cells (PSCs) meet the efficiency criteria for market implementation, there is a striking lack of stability studies needed for technology industrialization [13-21].

Alongside with solar irradiance, temperature is probably the most important outdoor variable that affects the conversion efficiency of PV devices. However, temperature studies on DSCs are scarce and usually limited to temperatures up to 60 ºC [22-28]. Moreover, the glass substrates normally used to assemble DSCs are poor thermal conductors, resulting that real temperature value are usually lower than anticipated by typical temperature control setups; solar simulators irradiance also increase the glass temperature (absorbance of *ca*. 20 %), which makes it difficult to have a good control over the temperature analysis. To the best knowledge of the authors, all reported studies have not considered these effects and should lack of accuracy making our knowledge on the temperature effect on DSCs performance just qualitative.

Generally, conduction band shift of the TiO_2 film, recombination and charges transport kinetics are in a DSC the phenomena that have the greatest contribution for its performance dependence on the temperature [22, 26-28]. Charge recombination corresponds to the undesirable reaction of generated electrons with electrolyte species, ultimately ruling the final performance of DSCs. This reaction involves either free conduction band electrons or electrons trapped in lower energy states [29]. Electronic traps are sites within the semiconductor (energetically localized in the bandgap) that restrict the movement of electrons. They are caused either by chemical impurities, morphological defects or imperfections in the regular spacing of the atoms [30]. The driving force for recombination is related to the energy level where electrons are located in the TiO_2 and temperature, both related to the rate constant, $k_r(T)$, and the electron concentration [31, 32]. As V_{OC} changes, the Fermi level (E_F) in TiO_2 moves towards or away from the conduction band edge (E_{CB}); when the Fermi level moves up, the respective electron traps below are filled. Taking this into consideration, it can be expected that the activation energy (E_a) of recombination is proportional to (E_{CB}-E_F)[33]. However, recombination processes do not take place only at TiO_2/electrolyte interface; they can occur by reaction of electrolyte species with generated electrons that can be located either in the TiO_2 photoelectrode or in the transparent conductive oxide (TCO) – Figure 1. This information is well known in the DSC community, and several passivation methodologies have been developed to decrease recombination [34-39]. The most successful strategies include the use of blocking layers over the TCO film [37, 38, 40-42]; the use of TiO_2 sols applied to the mesoporous TiO_2 layer [43, 44]; and more recently the use an encapsulation layer by atomic layer deposition (ALD)

of TiO_2 applied over the dyed semiconductor [39]. These approaches were developed to prevent recombination by different mechanisms, and although proved effective, studies that link temperature effects with recombination rates are rare.
Usually the recombination kinetics is well characterized by electrochemical impedance spectroscopy (EIS) and its magnitude can be analysed by fitting the experimental data to appropriate electrical analogues. [45, 46]. The electron lifetime (τ_{e^-}) can be extracted and thus the recombination rate constant ($k_r=1/\tau_{e^-}$) in the solar cell can be calculated. This powerful analytical technique has proven invaluable during the DSC technological development; unfortunately, *per se*, it does not allow distinguishing different recombination reaction pathways, *i.e.* at TiO_2 or SnO_2-F interface – Figure 1b).
The present work aims understanding and quantifying the recombination at TiO_2/electrolyte and FTO/electrolyte interfaces and their dependence with temperature. This should provide valuable information for the development of more efficient materials, solar cell architectures and to better predict temperature influence on PV output of future commercial applications. An experimental setup was developed that accurately controls the inner temperature of DSC devices, allowing their characterization as a function of the temperature. Laser assisted glass sealing, reported elsewhere [47, 48], was used to make the solar cells hermetic, even up to the boiling point of the electrolyte; the setup and sealing process allows obtaining very accurate characterizing results between set points of -5 ºC and 105 ºC. The temperature influence in *I-V* curves as well as in the electrochemical kinetics of the solar cell were determined and are discussed. It was

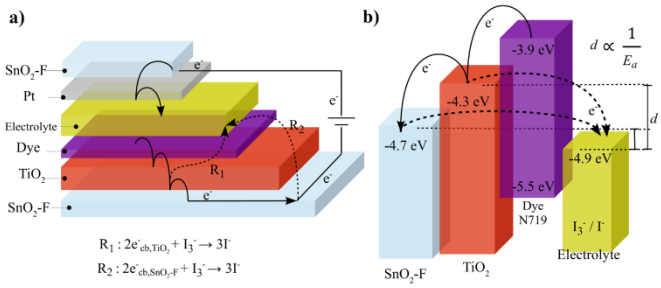

Fig. 1 a) Schematic representation of the working principles at a dye sensitized solar cell; and b) diagram of energy levels of each functional layer in the DSC. The full arrows represent electron pathways through the device; the dashed arrows represent the main loss reaction mechanisms due to recombination through TiO_2 or SnO_2-F interfaces (R_1 and R_2, respectively). The actual energy levels may change upon assembling.

developed an experimental methodology that distinguishes the recombination occurring at TiO_2/interface from recombination occurring at TCO (SnO_2-F) interface; to do so the exposed TCO area to electrolyte was progressively increased to deliberately cause changes in the recombination rate constant. This allows quantifying the temperature influence for both recombination pathways and its implications in solar cells operation and respective architecture design.

2. Materials and Methods

Laser sealed DSCs and half-cell fabrication

In the present work two types of devices were fabricated: DSCs and half-cells – Figure 2 and Figure S1. DSCs are made of two electrodes: the photo electrode (PE) and the counter electrode (CE); the electrolyte in between contains the iodide/triiodide redox pair. PE and CE are each applied on glass coated with a transparent conducting oxide (TCO); the PE includes a mesoporous TiO_2 film sensitized with a dye responsible for light absorption. The CE consists of a nanometric platinum layer applied on the TCO surface and responsible for catalysing the reduction of triiodide to iodide. A half-cell configuration consists of two identical TCO glasses coated with the relevant material, separated the electrolyte. They mimic the phenomena in a DSC allowing evaluating the CE and electrolyte behaviours without the interference of the sensitized porous TiO_2 layer; in the present work they are used to study the electrochemical reaction of electrons with electrolyte species over a specific interface. Half-cells made with thin films of SnO_2-F, Pt, and TiO_2 were assembled to study the recombination reaction as a function of temperature. The preparation of both devices (DSCs and half-cells) is described as follows.
Photoelectrodes were prepared on 2.2 mm thick, 7 Ω/□ SnO_2-F (FTO) coated glass substrates from Solaronix®. First, the glasses were washed sequentially with a detergent solution (Alconox®, VWR) in an ultrasonic cleaner (Amsonic TTC) at 55 ºC for 15 min, followed by ultrasonic cleaning in deionized water at room temperature, rinsed with ethanol and dried

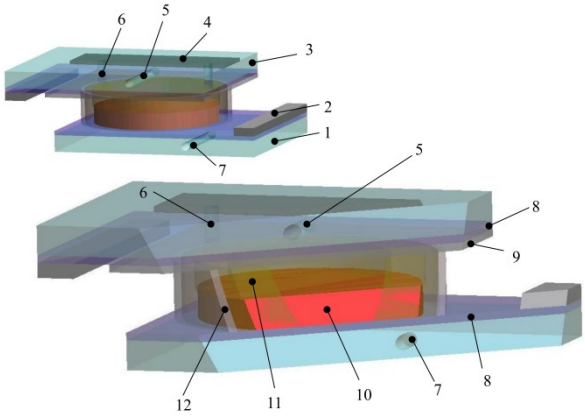

Fig. 2 Schematics of the manufactured DSC device (not in scale): 1 – Photoelectrode glass; 2 – electrical contact; 3 – counter-electrode glass; 4 – filling hole cover; 5 – drilled hole for temperature measurement, T_2; 6 –filling hole; 7 – drilled hole for temperature measurement, T_1; 8 – TCO; 9 – platinum catalyst; 10 – TiO_2 with adsorbed sensitizer; 11 – electrolyte; 12 – glass frit sealing.

with air at 50 ºC. Then, samples were coated with a porous TiO_2 layer by screen-printing a commercial TiO_2 paste (Ti-Nanoxide T/SP from Solaronix®), followed by drying at 100 ºC for 5 minutes. To control the final thickness of the transparent layer of TiO_2, the screen-printing and drying procedures were repeated as necessary to get the desired thickness (12 µm-thick photoelectrodes were obtained with three screen-printing cycles). Samples were annealed at 475 ºC for 15 min in an infrared electrical oven (Nabertherm Gmbh model GF75). After firing, the samples were treated with a 40 mM $TiCl_4$ aqueous solution at 70 ºC for 20 minutes, before being sintered at 475 ºC for 30 min. In cells where blocking layer is required, a thin and compact layer of TiO_2 above the FTO layer was applied immersing the FTO glasses in a 40 mM $TiCl_4$ aqueous solution at 70 ºC for 20 minutes; after washing with water and ethanol, the samples were dried with a nitrogen flow. The counter electrodes, prepared on the same type of glass substrates and cleaned as described before, were drilled previously with two holes of 1 mm diameter. A commercial platinum based paste (Platisol T/SP from Solaronix®) was applied on the glass substrate by screen-printing followed by annealing at 400 ºC for 15 minutes.

Both in DSCs and half cells devices, the two electrodes were assembled and sealed using a laser assisted glass frit method [47]. To control the exposed SnO_2-F area to electrolyte, the glass frit-sealing perimeter was varied from 5 to 12 mm (see Figure 11), without changing the total distance to the electrical contact; this way the electron lifetime can be controlled without changing the series resistances. Dye adsorption in the porous TiO_2 photoelectrode was obtained by recirculating a dye solution (0.5 mM N719, 5 M chenodeoxycholic acid in ethanol) for 12 hours using a peristaltic pump (Ismatec®, Reglo Digital MS-4/8), followed by ethanol rinsing, nitrogen drying, electrolyte filling (high stability iodolyte Z-150 from Solaronix®) and hole sealing by a combination of thermoplastic sealant (Surlyn®, Dupont) and high temperature resistant resin (Pattex® Nural 22 from Henkel). Solder bus bars and electrical wires were applied to the FTO surface of the photo and counter-electrodes, respectively, using an ultrasonic soldering unit (MBR electronics model USS-9210); the soldered bus bars were protected by high temperature resistant resin to prevent corrosion caused by the heat and moisture. The described manufacture process produced devices resistant at least to 120 ºC, without electrolyte leakage. The DSCs manufactured have an energy efficiency between 5 % and 6 % (25ºC, 100 mW·cm^{-2}, 1.5 air mass filter) which is typical for devices prepared with a non-volatile electrolyte (Iodolyte Z150 –Solaronix) based on methoxypropionitrile (MPN), known to produced stable but less efficient devices than with acetonitrile based electrolytes.

Experimental Setup

The experimental *I-V* characteristics were obtained in a setup equipped with a 150 W xenon light source (Oriel class A solar simulator, Newport, USA) with variable light intensity, from 10 to 100 mW·cm^{-2} (0.1 to 1 sun light intensity), and using a 1.5 air mass filter (Newport, USA). The simulator was calibrated using a single crystal Si photodiode (Newport, USA). The *I-V* characteristics of the solar cell were obtained applying an external potential load and measuring the generated photocurrent using an AUTOLAB electrochemical station. This station was also used to characterize the cells through EIS. The frequency range for EIS measurements was from 100 kHz to 0.05 Hz with an AC modulation signal of 10 mV. EIS measurements were carried out in dark and at the open circuit potential measured at 25ºC (V_{OC}, 25ºC) for DSCs and at 0 V for half-cells. The operation temperature of the solar cell was controlled using an in-house made experimental setup, shown in Figure 3 and Figure S2, based on a peltier device (Marlow Industries, model RC12-6) connected to a Keithley DC power supply (Model 2425C). A PID algorithm was run on a National Instruments LabVIEW application. Four K-type thermocouples were placed in different locations: in a drilled axial hole in the photoelectrode glass (T_1), in the counter electrode glass (T_2) and at aluminum slabs connected to the cold and hot side (T_3 and T_4, respectively) of the thermo-electrical element (peltier module). All heat transfer interfaces were filled with thermal conducting paste to maximize the heat transfer. When a potential difference is applied to the thermo-electrical element (4), a temperature difference is created between both sides (T_3 and T_4) of the peltier device.

By using a PID algorithm it is possible to accurately control temperature at the DSC (T_3). The heat-dissipating surface (T_4) of the peltier device was cooled using a thermal fluid from a thermostatic bath (Julabo model ME, Germany) (5). Under illumination, and without temperature control, the temperature inside the DSC can increase more than 10 ºC in a few minutes. Figure S3 presented in the supporting information shows that when the temperature control is turned on, the system immediately responds to correct the temperature to the desired set-point.

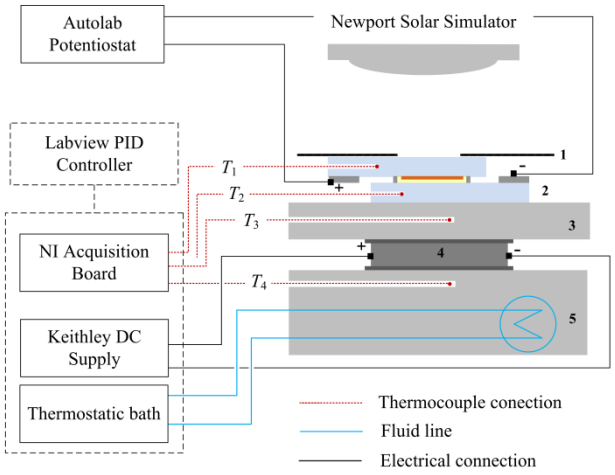

Fig. 3 Experimental setup used for temperature control of an under illumination DSC between -5 °C and 105 °C. 1- thermal insulator black mask; 2- DSC; 3- aluminum slab; 4- peltier device; 5- aluminum slab with drilled thermal fluid circuit.

Figure 4 show the temperature readings of a DSC device under illumination. Typically the temperature difference between the counter-electrode side (T_2) and the peltier cold side (T_3) is less than 1 ºC, as the heat conduction of the aluminium slab is quite high. However, the temperature difference between the glass substrates of both electrodes of the solar cell can be relatively high, especially at low or high temperatures. Above a set point of 50 ºC the temperature gap starts widening and it can go up to 20 ºC at 110 ºC; this illustrates the low thermal conductivity of the glass substrates.

Although the gap between both electrodes is filled with liquid electrolyte, there is always a temperature gradient inside the cell, particularly at temperatures far from room temperatures. This fact highlights the importance of taking correct temperature readings when analysing the temperature effect. In all results presented in this work the temperature was corrected to the average cell temperature calculated by the readings taken inside both glass electrodes of the solar cell (T_1 and T_2).

Results and Discussion

Temperature influence in DSC performance

I-V and EIS analysis were conducted in several batches of DSCs, from set point temperatures ranging from -5 ºC to 105 ºC. V_{OC}, J_{SC}, *FF* and η were read for each temperature using the average of three devices; these parameters were used to characterize the performance of the cells and are now on called performance parameters. The photoconversion efficiency (η) of the solar cell was determined by its current-voltage characteristics, specifically the open-circuit photovoltage (V_{OC}), the photogenerated current density measured under short-circuit conditions (J_{SC}), the intensity of incident light (I_s) and the fill factor of the cell (*FF*). The current and voltage output of the DSC result from a balance between charge generation flux and

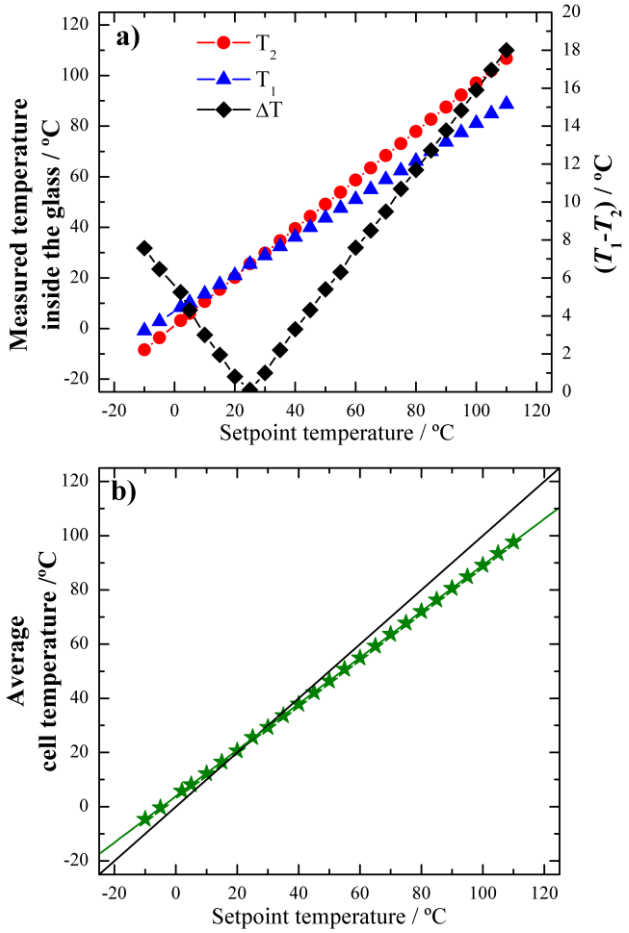

Fig. 4 Temperature values from: a) T_1 (photoelectrode), T_2 (counter electrode), calculated temperature difference between electrodes; and b) average cell temperature versus set point temperature.

recombination flux. The effect of temperature in the *I-V* curves of a typical DSC batch is presented in Figure 5. The *I-V* curves have been normalized with respect to V_{OC} and J_{SC} obtained at 25 ºC. As the temperature rises, there is a decrease in both V_{OC} and J_{SC} values, leading to a decrease in the performance. Figure 6 shows the performance parameters, normalized by the corresponding values obtained at 25 ºC, as a function of temperature. *FF* appears to be the only parameter that has some increase with temperature. It can be clearly seen that there are different decrease rates of V_{OC} and J_{SC} as a function of the temperature; the short circuit current has a higher decrease with temperature than the open-circuit voltage. *FF* is the ratio between the maximum power density and the product of V_{OC} and J_{SC}; because the V_{OC} decreases with temperature at a higher rate than J_{SC}, there is a higher *FF* for higher temperatures. In this particular batch of cells, the efficiency is approximately constant with temperature up to *ca*. 50 ºC. Considering 25 ºC as the reference temperature, at 50 ºC these cells retained about 91 % of the efficiency; at 70 ºC, 70 % and at 100 ºC, only *ca*. 30 %.

To check whether this loss of efficiency was reversible, the analysis was repeated at 25 ºC after the samples underwent the highest temperature analysis (Figure S1 and Table S1 in

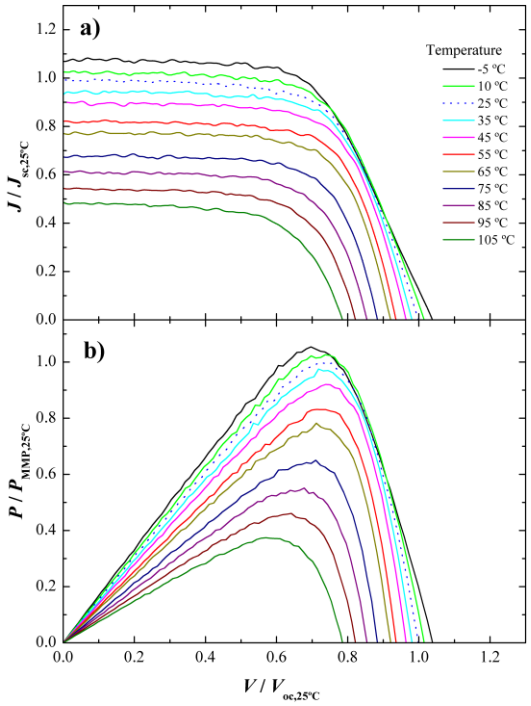

Fig. 5 (a) I-V and (b) power curves normalized to the corresponding values at 25ºC. as a function of the temperature.

supplementary information). The performance of DSCs showed excellent temperature resistance: there was a decrease in J_{SC}, but an increase in the *FF* that resulted in a higher efficiency (5.83 % *vs*. 6.01 % before and after the tests, respectively). The V_{OC} showed no meaningful changes (0.773 V vs 0.778V before and after the tests, respectively). The DSCs also showed less than 15 % total efficiency degradation after over 1000 hours of storage at room temperature in dark conditions, after conducting the temperature tests – Figure S2.

This was mainly due to a decrease in the J_{SC}, which in turn is probably caused by dye desorption from TiO_2 film occurred at high temperatures, a known phenomenon with the N719/I_3^- system [15, 21]; the V_{OC} and *FF* showed remarkable stability with

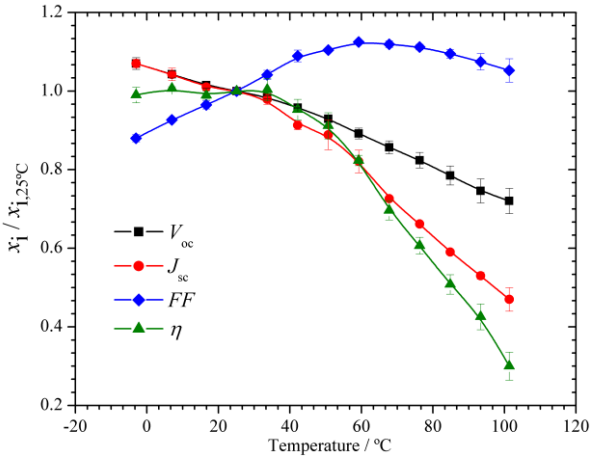

Fig. 6 Performance parameters normalized to the corresponding values 25 ºC values ($V_{OC,25ºC}$ = 0.77 V ; $J_{SC,25ºC}$ = 9.5 mA·cm^{-2}), as a function of the operating temperature. Lines were added for readability.

no particular degradation. These results show that, in the described analysis conditions and up to 100 ºC, there is no internal degradation of the solar cell components, which attests the thermal resistance and sealing quality of the prepared DSCs; this allows a correct analysis of the temperature influence.

The DSC efficiency dependence on the temperature is normally assigned to the conduction band shifts in the TiO_2 photoelectrode, recombination and charge transport processes [22, 48, 49]. Temperature controlled EIS experiments were conducted in platinum half cells, in order to characterize the temperature influence at the counter electrode during the operation of the DSCs. Bode and Nyquist diagrams are shown for platinum half cells in Figure 7, obtained at 0 V and under dark conditions for different

temperatures; the electrochemical reaction at the platinum catalyst layer and electrolyte was then assessed. The Bode diagram shows two frequency peaks, one at low frequencies, corresponding to the
diffusion of ionic species in the electrolyte (I^- and I_3^-), and another at high frequencies, ascribed to the electrochemical reaction at the platinum counter electrode with the electrolyte [50-52]. The operating temperature causes a slight frequency shift

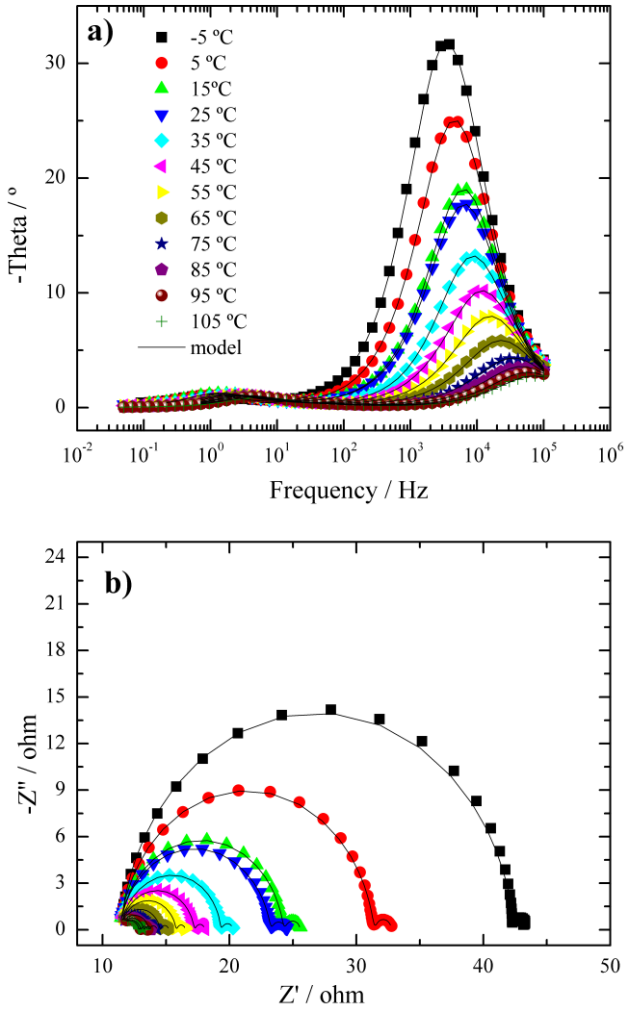

Fig. 7 Platinum half-cell Bode (a) and Nyquist (b) plots obtained in dark conditions at 0 V in in the temperature range -5 to 105 ºC.

in the low frequency peak, and a moderate shift in the high frequency peak, suggesting a higher temperature influence in the charge transfer process occurring at the Pt/electrolyte interface than in the electrolyte diffusion processes.
This behaviour is also observed in the Nyquist plot (Figure 7b): the first semicircle corresponds to the resistance associated to the electrochemical reaction of triiodide to iodide, and the second semicircle to the electrolyte diffusion in the liquid electrolyte. From the Nyquist plot it can be seen that the first semicircle changes considerably with temperature while the second semicircle changes only slightly. To understand and quantify this influence, the EIS experimental data was fitted to an equivalent electrical analogue based on a Randles-type circuit (presented in Figure S3), using ZView® (Scribner Associates Inc.) [53, 54]. The fitting results are shown in Figure 8, where the charge transfer resistance (R_{CE}), chemical capacitance of the counter electrode (C_{CE}), and ionic diffusion coefficient (D_{I3-}) are plotted against temperature. R_{CE} displays an exponential trend with temperature as expected from the Butler-Volmer equation; the electrolyte diffusion shows an exponential increase with temperature as well, whereas the counter electrode electrochemical capacitance remains relatively constant, unsurprisingly, as the reaction surface area is unchanged by temperature [55]. These results suggest that temperature has a highly beneficial effect regarding to the counter electrode operation. In DSCs, the electrochemical reaction at the counter electrode is basically the same that might happen at the photoelectrode when generated electrons undesirably react with electrolyte species present in the porous film of titanium dioxide; this prejudicial reaction, typically called recombination reaction, is believed to be the main limiting factor of efficiency, not only in DSCs but in the majority of solar technologies [56-58]. The fundamental difference between both reactions is the source of electrons and the interface where the electrochemical reactions take place. At the counter electrode the triiodide reduction reaction takes place catalysed by platinized layer applied on the SnO_2-F substrate; iodine diffuse then to the photoelectrode for regenerating the oxidized dye.

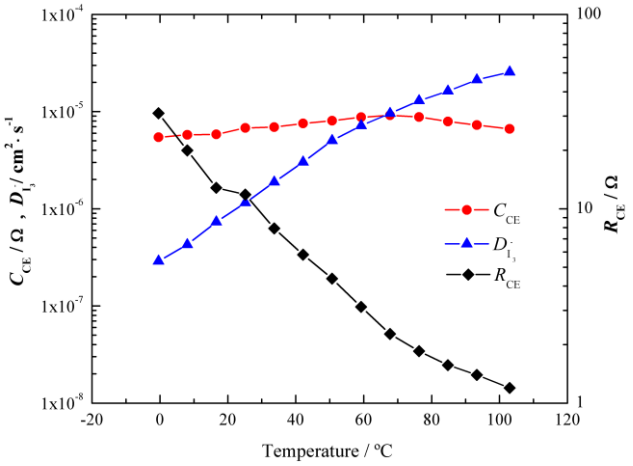

Fig. 8 Impedance data obtained for a platinum half-cell, at 0 V in dark conditions cells in the temperature range studied. Lines were added for readability.

Direct reduction of triiodide may happen at the photoelectrode – external recombination, which limits the total current and voltage and thus the final efficiency of the device. The recombination reaction can occur directly at TiO_2/electrolyte interface (R_1) or at the FTO/electrolyte interface (R_2), as represented in Figure 1.

Figure 9 shows for a typical batch of DSCs the EIS results. The experimental data was fitted using appropriated electrical analogues, namely using the transmission line model (presented in Figure S4) [59-61]. This model, proposed by Bisquert *et al.*[44], is widely used to describe the transport and recombination kinetic processes in DSCs. The experiments were conducted under dark conditions at the V_{OC} value obtained at 25 ºC (0.77 V). The Bode diagram shows two frequency peaks, corresponding to the electron transport and recombination at the photoelectrode (low frequency) and to the reduction reaction occurring at the platinum counter electrode (high frequency). Both phase peaks shift to higher frequencies as temperature increases; the shift of the high frequency peak in the Bode diagram and the first semicircle in the Nyquist plot teaches that the counter electrode performance improves with temperature.

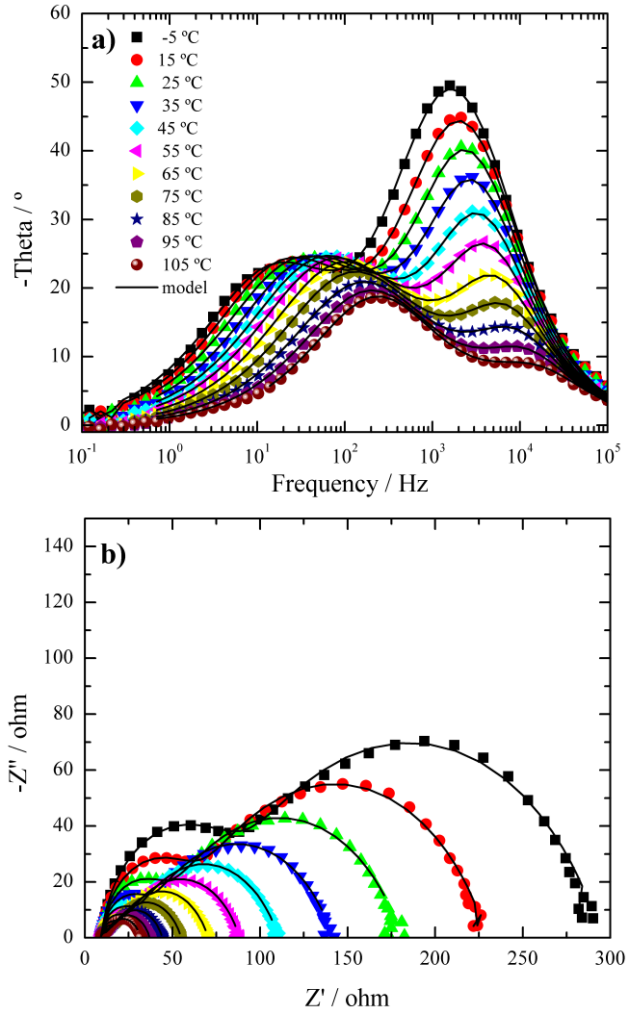

Fig. 9 Complete DSC Bode (a) and Nyquist (b) plots obtained under dark conditions, at the VOC of the cell at 25 ºC (-0.78 V) for the temperature range of 5 °C to 105 ºC.

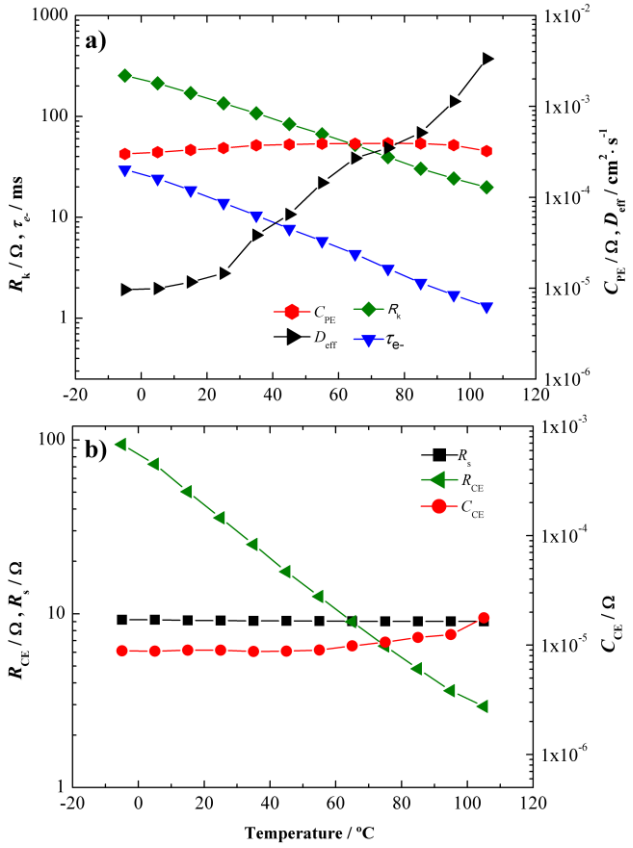

Fig. 10 Impedance parameters obtained by EIS for complete DSCs cells at 0.78 V under dark conditions, for the temperature range studied. Lines were added for readability.

Looking at the low frequency peak in the Bode diagram (Figure 9a) and the second semicircle in the Nyquist plot (Figure 9b) it appears that the electron/electrolyte recombination resistance decreases with temperature. The calculated parameters from the model fitting [60] are plotted against temperature in Figure 10. Transport and recombination related parameters are the photoelectrode capacitance, C_{PE}, electron diffusion coefficient, D_{eff}, recombination resistance, R_k, and electron lifetime, τ_{e^-}. While C_{PE} appears to be relatively constant, due to the unchanged reaction surface area, R_k and τ_{e^-} decrease exponentially with temperature.

This highlights the fact that the recombination reaction is highly enhanced by temperature. However, electron transport, evaluated by D_{eff}, improves with temperature. Considering that the final performance of the solar cell is a balance between electron generation, recombination and transport, there are two opposite effects caused by temperature: on one hand the recombination increases with temperature; however, the electron transport rate also increases with temperature. Assuming that electron generation rate, conduction band and electrolyte redox potentials are mostly constant with temperature[27], in terms of DSC performance clearly the balance is negative as seen from the global efficiency *vs*. temperature results (Figures 5 and 6). This highlights that, in terms of temperature dependence, recombination is dominant over the charge transport.

Recombination and DSC performance as a function of the temperature

To assess the recombination rate at interfaces TiO_2/electrolyte and FTO/electrolyte of the solar cell and their temperature dependence, five batches of DSCs were prepared and analysed by means of *I-V* and EIS characterization. Each batch, of three identical cells, differs in terms of total recombination rate constant, k_r(i). To experimentally change the total recombination reaction rate constant, k_r(1) to k_r(5), the perimeter length of the glass frit sealing was varied as displayed by Figure 11a); all the remaining solar cell design parameters (such as TiO_2 active area, distance to metallic contacts, etc.) were kept constant. This way it is possible to change the extent of free TCO area in contact with electrolyte, and thus the amount of generated electrons that may recombine with triiodide. It should be emphasized that the total distance from the active area to the metallic contact remains constant; therefore the series resistance in the solar cell is also constant between batches. Because the TiO_2/electrolyte interface is constant for all five batches of cells, it is then possible to assess the temperature effect on the recombination rate constant at the FTO/electrolyte.

Figure 11b) plots the electron lifetime against the exposed electrolyte area for DSCs with and without TiO_2 blocking layer. Indeed, the exposed area affects recombination,

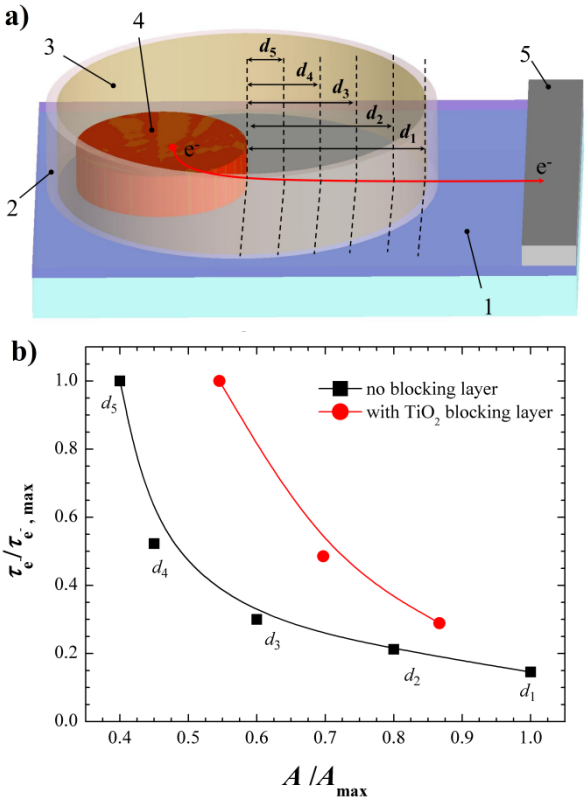

Fig. 11 a) Schematic diagram showing the methodology to control the FTO/electrolyte exposed reaction interface in the photoelectrode; 1 – TCO; 2 – glass frit sealing; 3 – electrolyte; 4 – TiO_2 with adsorbed sensitizer; 5 – electrical contact; the dashed lines represent the relative positioning of the glass fir sealing. b) Experimental results of electron lifetime versus exposed area of electrolyte to FTO or TiO_2 blocking layer. Lines were added for readability.

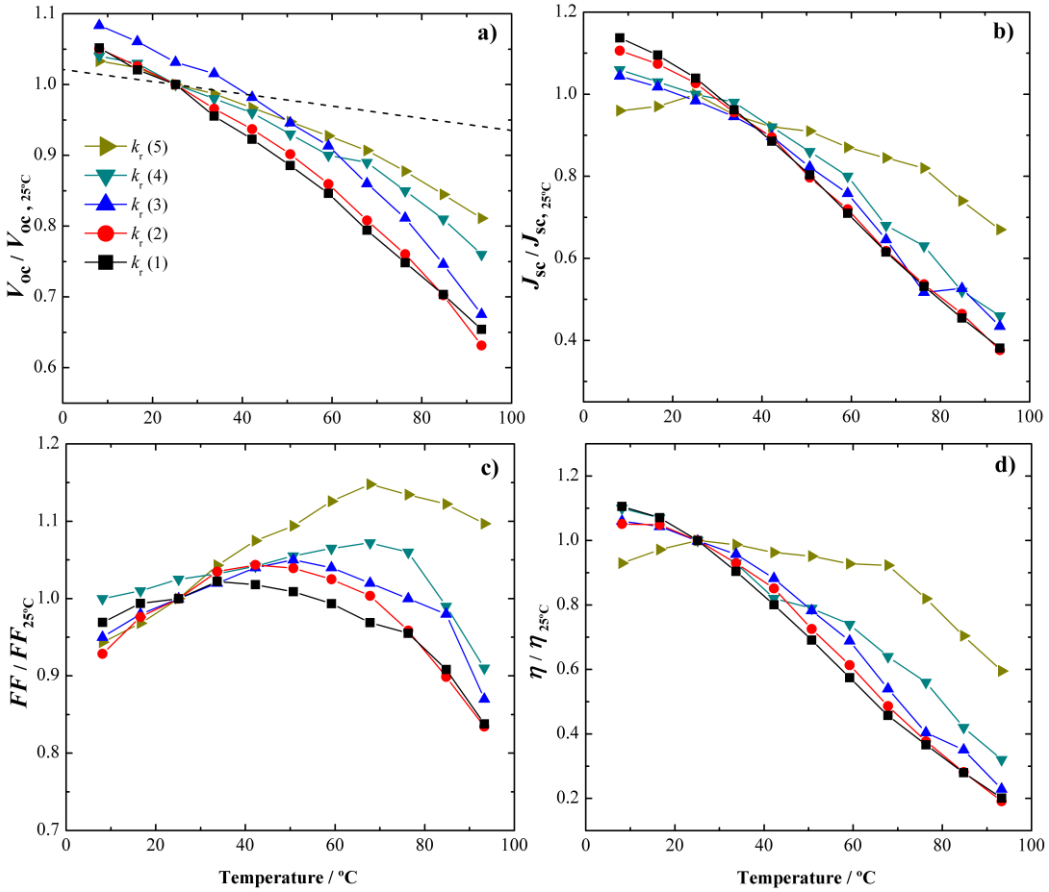

Fig. 12 *I-V* performance parameters relative to 25 ºC values of five different batches of DSCs differing in the recombination reaction constant $k_{r(i)}$.The black dashed line in a) corresponds to the theoretical V_{OC} *vs*. temperature trend expected for a cell with no recombination (calculated from the Butler-Volmer equation[64]). Lines were added for readability.

even in the case of DSCs with TiO_2 blocking layer applied over the SnO_2-F film. This illustrates the importance of minimizing the exposed non-active area to electrolyte, as well as the optimization of blocking layer design. An ideal blocking layer should completely prevent recombination, fact that does not happen according to the results presented in Figure 11b). The blocking layer employed was applied by chemical bath deposition of aqueous $TiCl_4$ solution; although this is a common method when preparing high efficient DSCs, it is known that this procedure may produce a defected blocking layer.[33, 62]

Analysing the *I-V* parameters (normalized by results at 25 ºC) for the different DSC batches, Figure 12, it is possible to conclude that the trend of each parameter (V_{OC}, J_{SC}, *FF* and η) depends on the total recombination rate constants; the rate constants were numbered from the highest, $k_r(1)$, to the lowest $k_r(5)$. The results indicate that the total recombination reaction rate increases monotonously with interface area and temperature. This means that even though the prepared solar cells at 25 ºC have similar efficiencies (~ 5 % to 6%), when subjected to different operating temperatures, substantial changes in performance emerge. The differences observed in the FF and efficiency are caused by V_{OC} (T) and J_{SC} (T) values. On one hand, it is expected TiO_2 conduction band down shift to the electrolyte redox potential, reducing in this way the open circuit voltage; however, this shift causes only a slight change as seen in Figure 12a) (dashed black line, calculated from the Butler-Volmer equation [63]). The difference between the normalized open circuit potential values, V^*_{OC}, predicted by Butler-Volmer and the observed values was assigned to the recombination. On the other hand, J_{SC} is basically determined by the balance between electron generation and recombination. Assuming that the temperature has a negligible effect in the photon absorption and electron generation processes [64, 65], the trend observed in Figure 12b) should then be mainly attributed to recombination. It can be concluded that recombination has a preponderant influence in the V_{OC} and J_{SC} evolution with temperature.

The recombination rate constants of the five batches of DSCs were plotted against the inverse of temperature to construct the Arrhenius plot – Figure 13a). As expected, the curves corresponding to cells with higher recombination display higher recombination rates. There are clearly two different trends in each curve with a breaking point at *ca*. 40 ºC, which correspond to different activation energy values. The activation energies (E_a) were calculated for each batch of cells, based on two linear fittings.

The two E_a values for each batch corresponds to the temperature ranges below ($E_{a,lt}$) and above ($E_{a,ht}$) 40 °C. These values were plotted against the respective rate constants in Figure 13b. There are two important observations: i) for both temperature ranges, the activation energies increase with recombination rate; ii) $E_{a,lt}$ is lower than $E_{a,ht}$. This means that more efficient cells, *i.e*. with less recombination (lower k_r), have lower activation energy values. This fact can be explained as follows: in this work to obtain high recombination cells the exposed TCO interface to electrolyte was increased as previously described; this means that for high recombination cells (*i.e*., $k_r(1)$) most of the recombination interface is SnO_2-F. Oppositely, in low recombination cells (*i.e*., $k_r(5)$) there is nearly no FTO exposed, and the main recombination reaction proceeds at TiO_2 interface.

The results suggest that the driving force for the electrochemical reaction between electrons and triiodide is related not only with a reaction rate constant, $k_r(T)$, (that is temperature dependent) and chemical concentration of triiodide in electrolyte (that in this case is constant across devices), but also with the energy level of electrons. Given this, when electrons are in a higher energy level (*i.e*. TiO_2 CB, -4.2 eV[66]) the activation energy required for recombination is lower comparing with electrons in lower energy levels (*i.e*. SnO_2-F CB, -4.7 eV[66]). This support the results for the activation energies being lower for TiO_2 dominant cells compared with DSCs with largely exposed TCO. Indeed, these results clearly show that the activation energy barrier rules the recombination process.

Chemical reactions occasionally show an Arrhenius plot with two different linear trends at regions of low and high temperatures, respectively. Typically, this feature is associated with simultaneous and competing reactions or reaction mechanisms involving different activation energies [67], with one reaction being dominant depending on the temperature range. In the present case, to understand the two trends of the DSCs recombination reaction Arrhenius plot, half-cells of FTO (SnO_2-F), TiO_2 and platinum films were prepared and analysed as described before; the correspondent Arrhenius plot is shown in Figure 14. As expected the platinum half-cells show very high reaction rates since platinum is good catalyst for the reduction reaction of triiodide to iodide. The SnO_2-F / SnO_2-F half-cells show two clear distinct trends in the Arrhenius plot: between 30 °C - 40 ºC there is very little influence of temperature in the reaction rate, showing very small activation

energy in this temperature range. However, for temperatures higher than 40 ºC there is a good linear fit resulting in activation energy of 0.66 eV. Contrarily, in the case of TiO_2/TiO_2 half-cells, the Arrhenius plot does not show multiple trends and the calculated activation energy was found to be 0.47 eV.

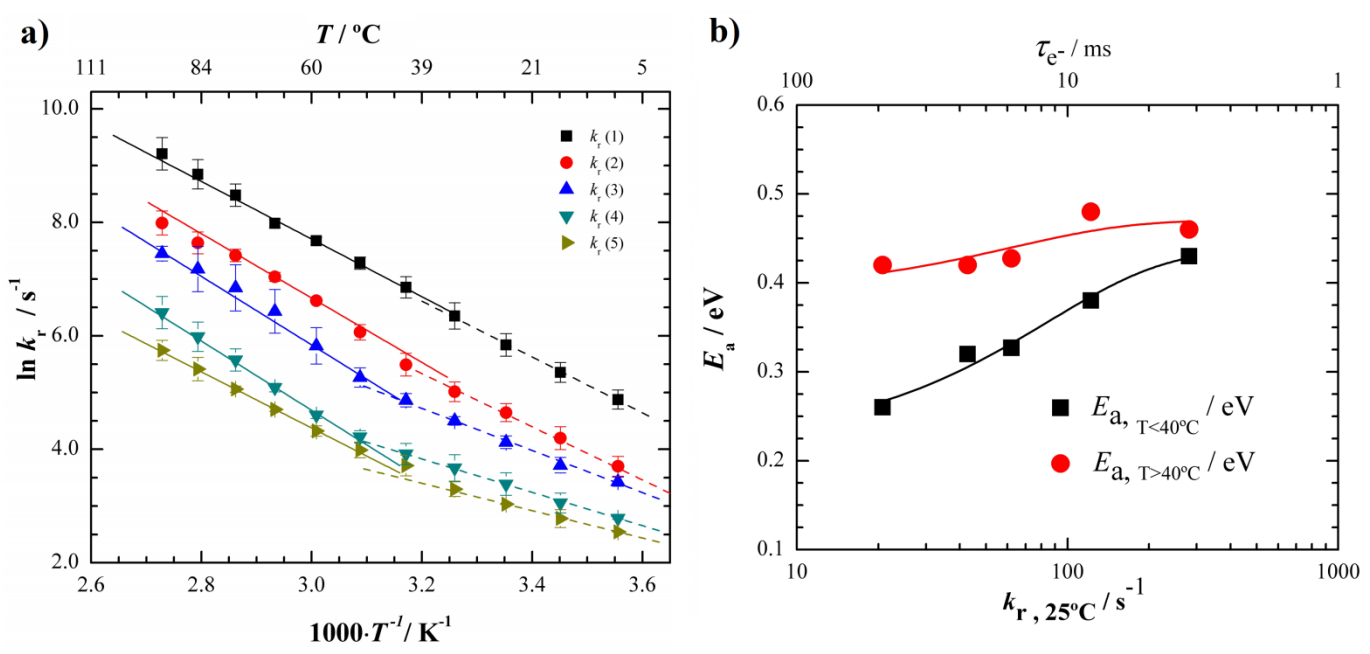

Fig. 13 a) Arrhenius plot, with respective linear fittings, for several sets of DSCs with different recombination rate constants; b) Activation energies *vs*. recombination rate constant and respective exponential fits, calculated from the Arrhenius plot trends found for temperatures lower and above 40 ºC. The calculated activation energies increase with recombination; an axis displaying the lifetime of electrons is also shown. Lines were added for readability

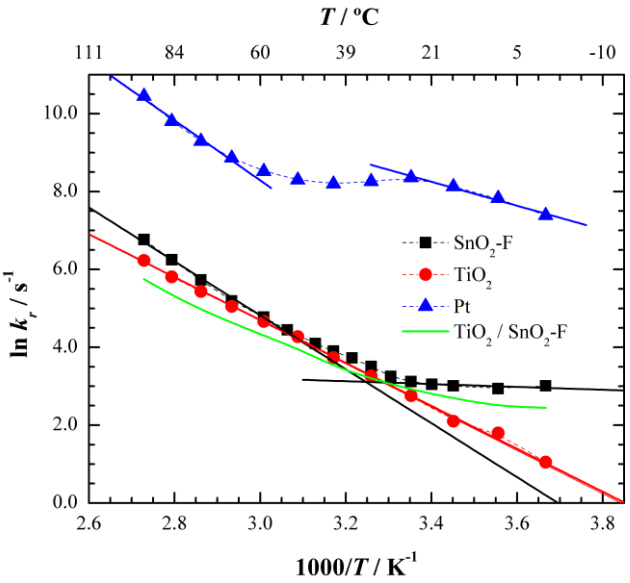

Fig. 14. Arrhenius plot of recombination reaction (reduction of triiodide) for three types of half-cells: SnO_2-F, TiO_2 blocking layer and Pt. The green curve represents the average between the TiO_2 and SnO_2-F curves.

To rationalize the shape of the Arrhenius plots for recombination in DSCs, seen in Figure 13a), the logarithmic of the average rate constants for SnO_2-F and TiO_2 was plotted -green curve in Figure 14. This has similar shape as the ones from complete DSCs, supporting that the influence that temperature has in the recombination process has a contribution from two distinct recombination mechanisms than can occur at the different interfaces of the solar cell.

The data presented at Figure 14 shows that at temperatures below 40 ºC, temperature has almost no influence in recombination reaction rate at the TCO interface. This suggests that at low temperature the main recombination reaction mechanism should be between trapped electrons and electrolyte. SnO_2-F trap states, located at energies below the conduction band, could be positioned close and even at lower energies than the redox energy of the electrolyte (energies from SnO_2-F CB and redox energy of electrolyte are close, c.a. -4.7 and -5.0 eV, respectively[66]), which means that below a certain temperature (40 ºC according to the results of this work) the reaction rate is mostly temperature independent, simply because most electrons do not have sufficient energy to react with the electrolyte. However, in the TiO_2 case, due to its higher conduction band energy (~-4.26 eV), most trap states ought to be located above the redox energy of the electrolyte. This means that, for the temperature range studied, most trapped electrons should have enough energy to react with electrolyte species.

The results suggest that there is a shift in the dominant recombination pathway from trapped electrons to electrolyte to CB electrons to electrolyte, which explains the different trends in the Arrhenius plots. The recombination reaction mechanism between CB electrons and electrolyte species requires less activation energy; this is confirmed by the activation energy values presented in Figure 13b). As the total recombination increases (higher k_r in abscissas axis of Figure 13b), activation requires progressively more energy due to the trapping energy.

The different shapes found in the Arrhenius plots of the platinum half cells can also be explained considering that the catalyst layer consists of platinum nanoparticles deposited on the TCO; SnO_2-F crystals exposed to electrolyte at this surface provide an alternative reaction pathway from the Pt catalyst.

Taking into account the above considerations, the main results concerning recombination *vs*. temperature are compiled in Table 1. The cells with low k_r show higher V_{OC} and higher activation energies for recombination reaction that occurs mainly at TiO_2 /electrolyte: $E_{a,lt}$ = 0.26 eV and $E_{a,ht}$ = 0.42 eV; when the main recombination interface is SnO_2-F/electrolyte (high k_r) the activation energy is found to be $E_{a,lt}$ = 0.43 eV and $E_{a,ht}$ = 0.46 eV.

Table 1. Recombination rate constants, open-circuit voltages at 25 ºC, and activation energies calculated for different batches of complete DSCs and half-cells.

Device		$k_{r,25ºC}$ / s^{-1}	$V_{oc,25ºC}$ / V	$E_{a,lt}$ / eV	$E_{a,ht}$ / eV
DSCs	$k_{r,(1)}$	281	0.719	0.43	0.46
	$k_{r,(2)}$	122	0.727	0.38	0.48
	$k_{r,(3)}$	62.1	0.734	0.33	0.43
	$k_{r,(4)}$	42.8	0.768	0.32	0.42
	$k_{r,(5)}$	20.8	0.770	0.26	0.42
Half-cells	Pt	4257		0.30	0.75
	SnO_2-F	22.64		0.0	0.66
	TiO_2	16.00		0.47	0.47

Conclusions

DSC performance as a function of the temperature was assessed for a wide range of temperatures, from -5 ºC up to 105 ºC. DSC cell were hermetically sealed using the recently developed laser assisted glass sealing process, which allowed obtaining reliable results. Within the temperature range considered, it was not observed degradation of the components of the solar cells, with full efficiency reversibility (at 25 ºC) in samples tested up to 100 ºC.

The recombination was quantified as a function of temperature and for SnO_2-F/electrolyte and TiO_2/electrolyte interfaces. It was concluded that the electrons energy level significantly affects the recombination reaction: when electrons are in a higher energy level (*i.e*. TiO_2 CB) the driving force for recombination is lower comparing with lower energy level electrons (*i.e.* SnO_2-F CB). Thus, the activation energy was found to be lower for the recombination taking place at TiO_2 interface than SnO_2-F interface with electrolyte (0.47 eV vs 0.66 eV, respectively).

Arrhenius plots for recombination rates in DSCs showed two different activation energies for temperatures below and above *ca*. 40 ºC. To explain this fact, the authors propose a shift in the dominant recombination pathway from trapped electrons/electrolyte to CB electrons/electrolyte. This work shows that recombination depends on both, the temperature and semiconductor interfaces present in the solar cell.

Generally temperature has an overall negative effect on the DSC performance; this effect was shown to be governed by the total electron/electrolyte recombination.

Acknowledgements

J. Maçaira is grateful to the Portuguese Foundation for Science and Technology (FCT) for his PhD Grant (Reference: SFRH/BD/80449/2011) and I. Mesquita acknowledges to Project WinDSC SI&IDT (ref. 21539/2011) for financial support. L. Andrade acknowledges European Research Council (Contract no: 321315). This work was financially supported by: Project UID/EQU/00511/2013-LEPABE, by the FCT/MEC with national funds and when applicable co-funded by FEDER in the scope of the P2020 Partnership Agreement; Project NORTE-07-0124-FEDER-000026-RL1_Energy, by FEDER funds through Programa Operacional Factores de Competitividade – COMPETE, by the Programa Operacional do Norte (ON2) program and by national funds through FCT - Fundação para a Ciência e a Tecnologia (PTDC/EQU-EQU/120064/2010). Financial support by European Research Council (Contract no: 321315) is also acknowledged. The authors would like to acknowledge the fruitful suggestions by reviewer #1, namely concerning the discussion on the recombination mechanisms.

References

1 H. Ossenbrink, T. Huld, A. J. Waldau and N. Taylor, Photovoltaic Electricity Cost Maps, 2013.
2 L. M. Goncalves, V. d. Z. Bermudez, H. A. Ribeiro and A. M. Mendes, Energy & Environmental Science, 2008, 1, 655-667.
3 M. K. Nazeeruddin, E. Baranoff and M. Grätzel, Solar Energy, 2011, 85, 1172-1178.
4 M. Grätzel, Journal of Photochemistry and Photobiology C: Photochemistry Reviews, 2003, 4, 145-153.
5 M. Ye, X. Wen, M. Wang, J. Iocozzia, N. Zhang, C. Lin and Z. Lin, Materials Today, 2015, 18, 155-162.
6 Y. Chiba, A. Islam, R. Komiya, N. Koide and L. Han, Applied Physics Letters, 2006, 88, 223505-223503.
7 Y. Chiba, A. Islam, Y. Watanabe, R. Komiya, N. Koide and L. Han, Japanese Journal of Applied Physics, Part 2: Letters, 2006, 45, L638-L640.
8 M. A. Green, K. Emery, Y. Hishikawa, W. Warta and E. D. Dunlop, Progress in Photovoltaics: Research and Applications, 2015, 23, 1-9.

9 A. Yella, H.-W. Lee, H. N. Tsao, C. Yi, A. K. Chandiran, M. K. Nazeeruddin, E. W.-G. Diau, C.-Y. Yeh, S. M. Zakeeruddin and M. Grätzel, Science, 2011, 334, 629-634.
10 J. Burschka, N. Pellet, S.-J. Moon, R. Humphry-Baker, P. Gao, M. K. Nazeeruddin and M. Gratzel, Nature, 2013.
11 N. J. Jeon, J. H. Noh, W. S. Yang, Y. C. Kim, S. Ryu, J. Seo and S. I. Seok, Nature, 2015, 517, 476-480.
12 H. Zhou, Q. Chen, G. Li, S. Luo, T.-b. Song, H.-S. Duan, Z. Hong, J. You, Y. Liu and Y. Yang, Science, 2014, 345, 542-546.
13 F. O. Lenzmann and J. M. Kroon, Advances in OptoElectronics, 2007, 2007, ID 65073.
14 N. Kato, Y. Takeda, K. Higuchi, A. Takeichi, E. Sudo, H. Tanaka, T. Motohiro, T. Sano and T. Toyoda, Solar Energy Materials and Solar Cells, 2008, In Press, Corrected Proof.
15 N. Kato, K. Higuchi, H. Tanaka, J. Nakajima, T. Sano and T. Toyoda, Solar Energy Materials and Solar Cells, 2011, 95, 301-305.
16 K.-M. Lee, C.-Y. Chen, S.-J. Wu, S.-C. Chen and C.-G. Wu, Solar Energy Materials and Solar Cells, 2013, 108, 70-77.
17 M. Flasque, A. N. Van Nhien, J. Swiatowska, A. Seyeux, C. Davoisne and F. Sauvage, ChemPhysChem, 2014, 15, 1126-1137.
18 D. Högberg, B. Soberats, S. Uchida, M. Yoshio, L. Kloo, H. Segawa and T. Kato, Chemistry of Materials, 2014, 26, 6496-6502.
19 G. Niu, X. Guo and L. Wang, Journal of Materials Chemistry A, 2015.
20 T. C. Sum and N. Mathews, Energy & Environmental Science, 2014, 7, 2518-2534.
21 N. Jiang, T. Sumitomo, T. Lee, A. Pellaroque, O. Bellon, D. Milliken and H. Desilvestro, Solar Energy Materials and Solar Cells, 2013, 119, 36-50.
22 S. R. Raga and F. Fabregat-Santiago, Physical Chemistry Chemical Physics, 2013, 15, 2328-2336.
23 M. Toivola, L. Peltokorpi, J. Halme and P. Lund, Solar Energy Materials and Solar Cells, 2007, 91, 1733-1742.
24 M. Berginc, U. Opara Krašovec, M. Jankovec and M. Topič, Solar Energy Materials and Solar Cells, 2007, 91, 821-828.
25 H. Yang, C. Yu, Q. Song, Y. Xia, F. Li, Z. Chen, X. Li, T. Yi and C. Huang, Chem. Mater., 2006, 18, 5173-5177.
26 K. Lobato and L. M. Peter, The Journal of Physical Chemistry B, 2006, 110, 21920-21923.
27 J. S. Henry, S.-M. Lukas, G. Michael and C. Marco, Physical Review B (Condensed Matter and Materials Physics), 2006, 74, 0453061-0453066
28 M. Wang, P. Chen, R. Humphry-Baker, S. M. Zakeeruddin and M. Gratzel, ChemPhysChem, 2009, 10, 290-299.
29 R. Memming, Semiconductor Electrochemistry, Wiley-VCH2001.
30 M. Bailes, P. J. Cameron, K. Lobato and L. M. Peter, The Journal of Physical Chemistry B, 2005, 109, 15429-15435.
31 B. O'Regan, L. Xiaoe and T. Ghaddar, Energy & Environmental Science, 2012, 5, 7203-7215.
32 B. C. O'Regan and J. R. Durrant, The Journal of Physical Chemistry B, 2006, 110, 8544-8547.
33 P. J. Cameron and L. M. Peter, The Journal of Physical Chemistry B, 2003, 107, 14394-14400.
34 L. Kavan, N. Tétreault, T. Moehl and M. Grätzel, The Journal of Physical Chemistry C, 2014.
35 L. Kavan, M. Zukalova, O. Vik and D. Havlicek, ChemPhysChem, 2014, 15, 1056-1061.
36 D. H. Kim, M. Woodroof, K. Lee and G. N. Parsons, ChemSusChem, 2013, 6, 1014-1020.
37 J. Xia, N. Masaki, K. Jiang and S. Yanagida, The Journal of Physical Chemistry B, 2006, 110, 25222-25228.
38 H.-J. Son, C. Prasittichai, J. E. Mondloch, L. Luo, J. Wu, D. W. Kim, O. K. Farha and J. T. Hupp, Journal of the American Chemical Society, 2013, 135, 11529-11532.
39 K.-I. Jang, E. Hong and J. Kim, Korean J. Chem. Eng., 2012, 29, 356-361.
40 C. Jiang, W. L. Koh, M. Y. Leung, W. Hong, Y. Li and J. Zhang, Journal of Solid State Chemistry, 2013, 198, 197-202.
41 W. Yongzhen, Y. Xudong, C. Han, Z. Kun, Q. Chuanjiang, L. Jian, P. Wenqin, I. Ashraful, B. Enbing, Y. Fei, Y. Maoshu, Z. Peng and H. Liyuan, Applied Physics Express, 2014, 7, 052301.
42 B. C. O'Regan, J. R. Durrant, P. M. Sommeling and N. J. Bakker, The Journal of Physical Chemistry C, 2007, 111, 14001-14010.
43 F. d. r. Sauvage, D. Chen, P. Comte, F. Huang, L.-P. Heiniger, Y.-B. Cheng, R. A. Caruso and M. Graetzel, ACS Nano, 2010, 4, 4420-4425.
44 J. Bisquert, The Journal of Physical Chemistry B, 2002, 106, 325-333.
45 J. Bisquert, Journal of Electroanalytical Chemistry, 2010, 646, 43-51.
46 F. Ribeiro, Maçaira,J. , Cruz, R., Gabriel, J., Andrade, L., Mendes, A., Solar Energy Materials and Solar Cells, 2012, 96, 43-49.
47 PCT/IB2012/051376, PCT/IB2012/051376, 2012.
48 A. Usami, S. Seki, Y. Mita, H. Kobayashi, H. Miyashiro and N. Terada, Solar Energy Materials and Solar Cells, 2009, 93, 840-842.
49 H. J. Snaith and L. Schmidt-Mende, Advanced Materials, 2007, 19, 3187-3200.
50 L. Andrade, J. Sousa, H. A. Ribeiro and A. Mendes, Solar Energy, 2011, 85, 781-793.
51 R. Cruz, D. A. Pacheco Tanaka and A. Mendes, Solar Energy, 2012, 86, 716-724.
52 F. Fabregat-Santiago, J. Bisquert, G. Garcia-Belmonte, G. Boschloo and A. Hagfeldt, Solar Energy Materials and Solar Cells, 2005, 87, 117-131.
53 R. Cruz, J. P. Araujo, L. Andrade and A. Mendes, Journal of Materials Chemistry A, 2014, 2, 2028-2032.
54 54.A. Hauch and A. Georg, Electrochimica Acta, 2001, 46, 3457-3466.
55 J. Bisquert, Physical Chemistry Chemical Physics, 2003, 5, 5360-5364.
56 H. J. Snaith, Advanced Functional Materials, 2010, 20, 13-19.
57 B. E. Hardin, H. J. Snaith and M. D. McGehee, Nat Photon, 2012, 6, 162-169.
58 J. Maçaira, L. Andrade and A. Mendes, Renewable and Sustainable Energy Reviews, 2013, 27, 334-349.
59 J. Bisquert, M. Gratzel, Q. Wang and F. Fabregat-Santiago, The Journal of Physical Chemistry B, 2006, 110, 11284-11290.
60 L. Andrade, S. M. Zakeeruddin, M. K. Nazeeruddin, H. A. Ribeiro, A. Mendes and M. Grätzel, ChemPhysChem, 2009, 10, 1117-1124.
61 Q. Wang, J.-E. Moser and M. Grätzel, The Journal of Physical Chemistry B, 2005, 109, 14945-14953.
62 B. Yoo, K.-J. Kim, S.-Y. Bang, M. J. Ko, K. Kim and N.-G. Park, Journal of Electroanalytical Chemistry, 2010, 638, 161-166.
63 J. Macaira, L. Andrade and A. Mendes, RSC Advances, 2014, 4, 2830-2844.
64 M. Grätzel, Progress in Photovoltaics: Research and Applications, 2000, 8, 171-185.
65 M. Grätzel and J.-E. Moser, in Electron Transfer in Chemistry, ed. V. Balzani, Wiley-VCH, Weinheim2001, vol. 5, ch. Part 3.
66 R. Memming, in Semiconductor Electrochemistry, Wiley-VCH Verlag GmbH2007, pp. 241-263.
67 L. Masgrau, À. González-Lafont and J. M. Lluch, Theor Chem Acc, 2003, 110, 352-357.